



AERODYNAMIC PARTICLE SIZE MEASUREMENT BY ELECTRODYNAMIC OSCILLATION TECHNIQUES

F. Zheng, M. L. Laucks and E. J. Davis*

Department of Chemical Engineering, University of Washington, Seattle, WA 98195-1750, U.S.A.

(First received 5 August 1999; and in final form 20 December 1999)

Abstract—Four dynamical techniques for measuring the aerodynamic size of spherical and non-spherical aerosol particles are evaluated and compared. For spheres the classical method of angular light scattering is also included. One method based on particle dynamics, the so-called springpoint method, has been extensively used, but the other particle oscillation methods have been used rarely or not at all. All the dynamical methods involve imbalancing a particle in an electrodynamic balance (EDB) by changing the dc potential to produce particle oscillation. A linescan CCD camera and associated electronics were used to measure the amplitude of the oscillations, the offset of oscillation centers, and the phase lag relative to the ac drive. These measurements are compared with theoretical solutions of the equation of particle motion to establish the aerodynamic size of the particle. The stability characteristics of the particle are analyzed by solving the particle equation of motion using the method of continued fractions. The various techniques are compared for spheres, spheroids and crystalline or amorphous particles of irregular shape. All five methods are shown to be in good agreement for spheres (within 3.9%). For non-spherical germanium dioxide particles the three oscillation methods agree with the springpoint method within 3.4%. © 2000 Elsevier Science Ltd. All rights reserved

INTRODUCTION

A variety of studies require information on the effective size and/or particle morphology of particles with irregular shapes. The present work grew out of the need to determine the aerodynamic size and shape of such particles involved with investigations of gas/particle chemical reactions, microparticle Raman spectroscopy and thermophoretic force measurements using electrodynamic levitation techniques. The thermophoretic force is particularly sensitive to the particle size or particle mobility.

Numerous methods have been proposed for single-particle size measurements since Millikan used his oil drop experiment to determine the droplet size by measuring its rate of fall and applying Stokes' law. Light-scattering measurements constitute the most effective way to size small spheres, and the first measurements of angular light scattering from a single sphere were reported by Gucker and Egan (1961) using a Millikan condenser to levitate a particle in a light beam. Blau *et al.* (1970) applied an electrodynamic balance (EDB) for the same purpose. Davis and Ray (1980) adapted an EDB to size evaporating droplets, and Davis and Periasamy (1985) introduced a laminar jet technique for determining the aerodynamic size of particles, which was shown to agree with light-scattering measurements when applied to spheres.

Springpoint measurements made in an EDB were introduced by Ataman and Hanson (1969) to determine the charge on a droplet at the Rayleigh limit of charge. Davis and his colleagues (Tafllin *et al.*, 1989; Rassat and Davis, 1992; Li and Davis, 1995; Aardahl *et al.*, 1997a, b; Swanson *et al.*, 1999) made many springpoint measurements to size particles and to determine the relevant balance constants for EDBs. The springpoint corresponds to a sudden large-amplitude oscillation of an electrostatically levitated particle when the ac field reaches a critical value that depends on the aerodynamic drag on the particle and other particle properties. The dynamics of a charged particle in an EDB were analyzed by

* Author to whom correspondence should be addressed: The Technical University of Vienna, Institute for Analytical Chemistry, C/o Prof. Dr. Hans Puxbaum, Getreidemarkt 9/151, 1060 Vienna, Austria.

Frickel *et al.* (1978), and Davis (1985) showed that the stability characteristics of the particle could be used to determine its aerodynamic size. Bar-Ziv and de Botton (1991) used the methods of Frickel and his coworkers and Davis to calculate the motion of a particle under feedback control.

Sageev *et al.* (1986) used a variation of Millikan's method to size particles by sedimentation in an electrodynamic balance, and Roll *et al.* (1996) developed a sedimentation technique based on optical trap measurements. The latter method involved a comparison between calculated and experimental particle positions as a function of time after the illuminating laser beam was interrupted. Optical levitation in a Gaussian beam is not useful for non-spherical particles because unbalanced lateral forces are exerted on the particle that prevent stable levitation. Maloney *et al.* (1995) generated transient particle trajectories in an EDB and compared measured trajectories with numerically calculated trajectories to size particles. They estimated the uncertainty in the fitting procedure to be less than $\pm 5\%$ for polystyrene latex (PSL) spheres.

Göbel *et al.* (1997) investigated the use of phase lag measurements to size droplets in a four-ring EDB, reporting an uncertainty of less than 6% in the size determination. They did not report results for non-spherical particles. In fact, very few studies of sizing single-non-spherical aerosol particles have been published apart from the many laser-Doppler measurements reported. The phase lag method appears promising for non-spherical particles, but particle rotation or particle re-orientation can introduce noise in the light-scattering measurements, and if the frequency of rotation is near the frequency of oscillation, special signal processing must be introduced.

In their analysis of particle motion in an EDB, Frickel *et al.* observed that the shift in the position of the center of oscillation of an unbalanced particle is related to the drag on the particle and the amplitude of such oscillations depends on the drag characteristics of the particle. Consequently, it is feasible to measure either the shift or the amplitude to determine the particle size.

It was the objective of this research to use particle oscillation methods to compare the various methods and to assess the accuracy with which particle sizes and drag characteristics can be measured. These measurements complement work on thermophoresis since it is necessary to know the particle size in the analysis of thermophoretic force data. The choice of particles was determined by the particles of interest there, particularly GeO_2 particles used in fiber optic production.

Theory

When Laplace's equation is solved for the ac field in an EDB, the vertical and radial components are found to be 90° out of phase, and in the vicinity of the nullpoint ($z = 0, r = 0$) the vertical component of the field strength is twice that of the radial component. Consequently, any initial instability occurs only in the vertical direction, and we need only write the z -component of the equation of motion to investigate the stability characteristics of a trapped particle. If the solutions of Laplace's equation for the ac and dc electrical fields in an EDB are linearized about the nullpoint of the balance, the non-dimensional vertical equation of motion is

$$\frac{d^2Z}{d\tau^2} + \delta \frac{dZ}{d\tau} - 2\beta Z \cos 2\tau = \sigma, \quad (1)$$

in which Z is the dimensionless distance from the nullpoint ($Z = z/b$), τ is the dimensionless time ($\tau = \omega t/2$), $\omega = 2\pi f$, where f is the ac frequency, and $b = z_0 C_0/C_1$ is a characteristic length scale that depends on the balance geometry. Here $2z_0$ is the distance between the electrodes, and C_0 and C_1 are the dc and ac balance constants, respectively, as defined by Davis (1985). The parameter b is obtained by calibration of the balance using a microsphere of known size and density. This was done by springpoint measurements.

The dimensionless parameters δ , β and σ are the drag parameter, the ac field strength parameter and the imbalance parameter, respectively, defined by

$$\delta = \frac{6\pi\mu d_p \kappa}{m\omega} = \frac{36\mu\kappa}{\omega d_p^2 \rho_p}, \quad (2)$$

$$\beta = \frac{2g}{\omega^2 b} \left(\frac{V_{ac}}{V_{dc,0}} \right), \quad (3)$$

and

$$\sigma = \frac{4g}{\omega^2 b} \left(\frac{V_{dc}}{V_{dc,0}} - 1 \right), \quad (4)$$

in which m is the particle mass, ρ_p its density, d_p is the diameter of a sphere that has the same volume and mass as the particle of interest, V_{dc} is the dc potential between the electrodes, $V_{dc,0}$ is the dc potential necessary to balance the particle weight, V_{ac} is the ac potential, κ is a dynamic shape factor that accounts for corrections to Stokes' law for non-spherical particles, μ is the gas viscosity, and g is the gravitational acceleration constant.

The drag force

Equation (2) arises from the assumption that the particle motion is in the Stokes' law regime and that the dynamic shape factor for non-spherical particles, κ , takes into account deviations from the sphere. The effective diameter or equivalent diameter, d_p , and κ can be calculated for a number of specific geometries as outlined by Laucks *et al.* (2000). We will apply the relationships for prolate and oblate spheroids for our data analysis, for the particles studied were approximately spheroidal and not at all chain-like.

The dynamic shape factor for a spheroid depends on its axis ratio, q , and its orientation in the flow field (Kasper, 1982; Oberbeck, 1876). For a spheroid, q is the ratio of the length of its axis of revolution to that of the other axis. We denote the particle orientation by the subscripts \parallel and \perp , in which \parallel indicates that the axis of revolution is parallel to the flow and \perp indicates that the spheroid's axis of revolution is perpendicular to the flow.

For prolate spheroids, $q > 1$, and the dynamic shape factors are given by

$$\kappa_{\parallel} = \frac{4}{3} \frac{(q^2 - 1)q^{-1/3}}{[2(q^2 - 1) + 1](q^2 - 1)^{-1/2} \ln[q + (q^2 - 1)^{1/2}] - q} \quad (5)$$

and

$$\kappa_{\perp} = \frac{8}{3} \frac{(q^2 - 1)q^{-1/3}}{[2(q^2 - 1) - 1](q^2 - 1)^{-1/2} \ln[q + (q^2 - 1)^{1/2}] + q}. \quad (6)$$

The volume of a prolate spheroid is

$$V_{\text{prolate}} = \frac{4}{3} \pi a^* b^{*2} = \frac{\pi}{6} d_p^3, \quad (7)$$

where a^* is the major semi-axis and b^* is the minor semi-axis.

For oblate spheroids ($q < 1$) the equivalent dynamic shape factors are

$$\kappa_{\parallel} = \frac{4}{3} \frac{(q^2 - 1)q^{-1/3}}{[2(q^2 - 1) + 1](1 - q^2)^{-1/2} \arccos(q) - q} \quad (8)$$

and

$$\kappa_{\perp} = \frac{4}{3} \frac{(q^2 - 1)q^{-1/3}}{[2(q^2 - 1) - 1](1 - q^2)^{-1/2} \arccos(q) + q}. \quad (9)$$

The corresponding volume of an oblate spheroid with major semi-axis a^* and minor semi-axis b^* is

$$V_{\text{oblate}} = \frac{4}{3} \pi a^{*2} b^* = \frac{\pi}{6} d_p^3. \quad (10)$$

If a non-spherical particle is approximated as a spheroid based on particle imaging, q can be estimated from the major and minor dimensions of the image, and the orientation of the particle in the EDB can be determined. Then the appropriate dynamic shape factor can be applied.

Solution of the equation of motion

Equation (1) may be written in an alternate form by introducing the transformation, $U = Z \exp(\delta\tau/2)$, to give

$$\frac{d^2U}{d\tau^2} + (\alpha - 2\beta \cos 2\tau)U = \sigma e^{\delta\tau/2}, \tag{11}$$

where $\alpha = -\delta^2/4$. If the dc potential is adjusted to balance the gravitational force ($\sigma = 0$), equation (11) reduces to the Mathieu equation

$$\frac{d^2U}{d\tau^2} + (\alpha - 2\beta \cos 2\tau)U = 0. \tag{12}$$

The Mathieu equation has an infinite set of stable and unstable regions in α - β space (or δ - β space). Müller (1960) obtained an approximate solution for the first boundary between stable and unstable domains in terms of δ and β , and the exact solution was determined by Frickel *et al.* using the method of continued fractions to solve the governing equation. The boundary between stable and unstable particle motion has been called the springpoint or marginal stability curve. In the unstable region large-amplitude oscillation occurs, and the particle can collide with the surface of the EDB.

Müller’s equation for the marginal stability state or critical value of β , above which instability occurs, is given by

$$\beta_{crit}^2 = \frac{1}{2}(99 + 3\delta^2) - \sqrt{\frac{1}{4}(99 + 3\delta^2)^2 - (1 + \delta^2)(81 + 9\delta^2)}. \tag{13}$$

The coefficients multiplying δ^2 in this equation differ from Müller’s original since his drag parameter was defined to be one-half of ours.

When the dc potential does not balance the gravitational force and β is less than its critical value the particle oscillates at the frequency of the ac source, and the particle trajectory can be obtained by solving equation (1). We have solved the equation by the method of continued fractions outlined by Frickel and his coworkers.

The general solution of equation (1) has the form

$$Z(\tau) = AZ_1(\tau) + BZ_2(\tau) + P(\tau), \tag{14}$$

where $Z_1(\tau)$ and $Z_2(\tau)$ are solutions of the homogeneous equation that decay to zero within a few oscillations when the particle undergoes stable oscillation ($\beta < \beta_{crit}$), and $P(\tau)$ is a periodic function that satisfies the inhomogeneous equation. The stable oscillation of a particle that occurs when $\sigma \neq 0$ is described by $P(\tau)$ after enough time has elapsed. The function $P(\tau)$ can be written as a Fourier series,

$$P(\tau) = \sum_{n=-\infty}^{\infty} a_n e^{2in\tau}. \tag{15}$$

If this Fourier series is substituted into equation (1), we obtain the recursion formulas,

$$r_n = \frac{\beta}{2(-2n^2 + in\delta) - \beta r_{n+1}}, \tag{16}$$

$$a_n = r_n a_{n-1} \tag{17}$$

and

$$a_0 = \frac{\sigma}{2\beta \Re(r_1)}, \tag{18}$$

in which $\Re(r_1)$ is the real component of the complex number, r_1 .

When the particle is in the stable region the series converges, and a sufficiently large N will satisfy $|\beta r_{N+1}| \ll |2(-2N^2 + iN\delta)|$. Thus, we may write

$$r_N = \frac{\beta}{2(-2N^2 + iN\delta)} \quad (19)$$

and calculate the ratios, r_n , from r_N recursively. The Fourier coefficients, a_n , up to order N can be calculated from the values of a_0 and r_n . As long as the particle oscillation is not close to the instability boundary, the higher-order terms in the Fourier series will be vanishingly small compared to a_0 and a_1 . This condition is easily satisfied in experiments, and in this case the particle oscillation can be represented by

$$z(t) = A_0 + A_1 \cos(\omega t + \theta). \quad (20)$$

in which A_0 represents the offset of the oscillation relative to the nullpoint of the balance, A_1 is the amplitude of the oscillation, and θ is the phase shift relative to the ac electric field. All of these parameters are measurable quantities. They are related to the Fourier coefficients by

$$A_0 = a_0 b = \frac{\sigma b}{2\beta \Re(r_1)}, \quad (21)$$

$$A_1 = 2|a_1|b = \left| \frac{\sigma r_1 b}{\beta \Re(r_1)} \right| \quad (22)$$

and

$$\theta = \arctan\left(\frac{\Im(r_1)}{\Re(r_1)}\right). \quad (23)$$

In principle, particle sizes can be determined from any one of these measurable quantities because they all depend on the complex number r_1 , which in turn depends on the drag parameter and, consequently, on particle size. Both the amplitude A_1 and the offset A_0 are linear with respect to the dc voltage, which simplifies data analysis. The phase lag, θ , is independent of the dc voltage except for the 180° phase reversal as the dc voltage is changed through the null point voltage and the particle changes its direction of oscillation. However, θ is sensitive to the ac frequency.

EXPERIMENTS

The electrodynamic balance used in this study was a modification of the double-ring device described by Li and Davis (1995). An overhead view of the experimental setup is shown in Fig. 1. Single particles were trapped at the midpoint between the two ring electrodes.

The particle position-sensor is a CCD linescan camera (Reticon). The camera has a single line of 256 pixels aligned in the vertical direction. The optical axis of the camera and its $9.45\times$ zoom lens is horizontal. Aligned to this optical axis is a horizontal He-Ne laser beam, which casts a shadow of the trapped particle on the camera. As the particle oscillates, its magnified shadow covers different groups of pixels at different times. The resulting pixel gray-scale profile is, therefore, time-dependent and can be integrated with respect to the pixel number to determine the particle position as a function of time.

Non-spherical particles of germanium dioxide (Atlantic Metals, Inc.) were used. The particle mean diameter stated by the manufacturer was $7\ \mu\text{m}$. These non-spherical particles were approximated as spheroids as discussed above. The shapes and orientations of these non-spherical particles were obtained using a standard video camera, which shared the zoom lens with the linescan camera. It was observed that by adjusting the frequency and the amplitude of the ac field to be close to the springpoint values, a non-oscillating particle could be made to rotate around its vertical axis, exposing its different sides to the

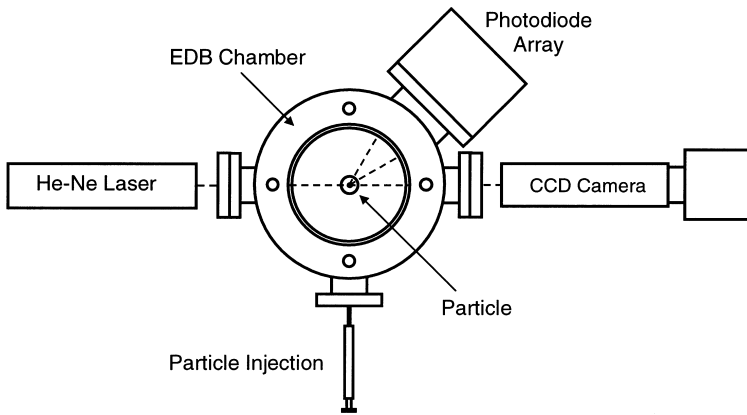


Fig. 1. Top view of the experimental apparatus. The linescan camera and the video camera share the same port.

video camera. Based on the images of the rotating particle, it could be decided whether the particle was better approximated as a prolate or oblate spheroid, and the axis ratios used in the dynamic shape factor calculations were determined from the images.

If the ac field strength is not near the springpoint, a spheroid trapped in the EDB tends to remain in a preferred orientation due to the non-uniformity in both the ac field and the particle shape. Prolate spheroids usually align such that the major axis is vertical, and oblate spheroids normally align with the minor axis horizontal. We observed that particles in stable oscillation preserve these preferred orientations. With the knowledge of the particle axis ratio and its orientation, the dynamic shape factor was calculated using the appropriate equation from equations (5), (6), (8) and (9).

Stable oscillation was initiated by changing the levitation dc voltage so that the particle weight was unbalanced. The oscillation trajectories were recorded at different dc voltages, and the offset, amplitude and phase lag of the oscillation were determined by Fourier transform of the position-time data. The equivalent-volume diameter of a particle was determined by comparing the oscillation characteristics with the continued fractions model, with the particle shape and orientation taken into account by the dynamic shape factor.

For spherical particles, the angular light-scattering pattern was recorded using a photodiode array mounted on one port of the EDB, and the particle diameter was determined by comparing the data with Mie theory.

RESULTS AND DISCUSSION

Particle position sensing

A sample linescan image sequence of an oscillating germanium dioxide particle is shown together with the extracted trajectory in Fig. 2. The particle was oscillating at 106.8 Hz and its equivalent-volume diameter was determined to be $11.8\ \mu\text{m}$ by springpoint measurements. The image sequence was recorded during a period of 65.5 ms and is composed of 256 line images, each having 256 pixels in the vertical direction. The pixel gray-scale profile in each image line was integrated with respect to the pixel number to calculate the center position of the particle. The calculated particle trajectory is also presented in Fig. 2. The oscillation amplitude, the offset and the phase lag were determined from the processed signal by Fourier transform.

Spherical particle size measurements

Figure 3 shows a comparison between Mie theory and the measured phase function (angular scattering intensity distribution) for a soda lime glass microsphere with a

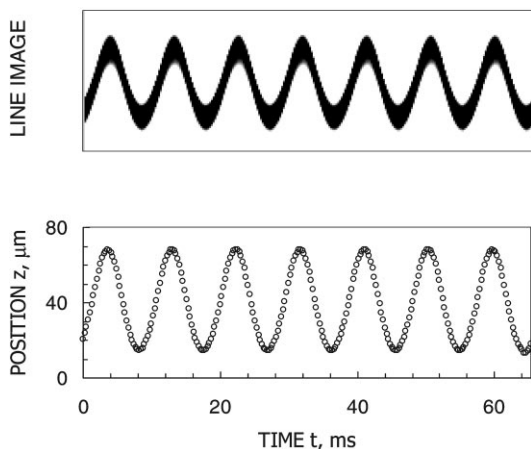


Fig. 2. Linescan image sequence and extracted oscillation trajectory for GeO_2 particle GDO926A.

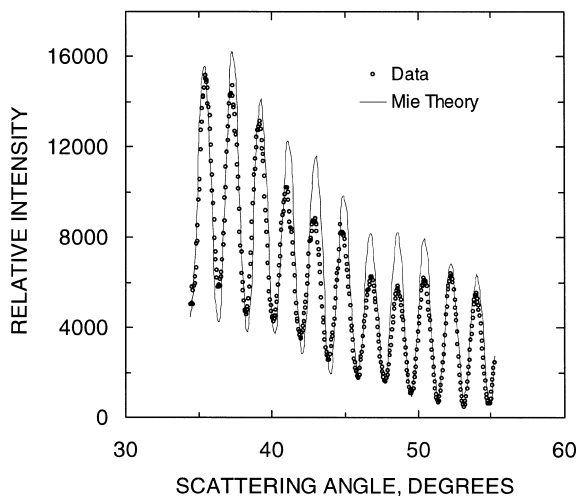


Fig. 3. Comparison of the measured phase function and Mie theory for glass sphere SLG914A.

manufacturer's nominal diameter of $21.9 \pm 1.4 \mu\text{m}$. The light-scattering diameter was determined to be $21.9 \pm 0.1 \mu\text{m}$. Noise in the phase function data is largely due to pixel-to-pixel variations in the sensitivity of the detector and to the dark current. The pixels were not calibrated, and the array was not cooled.

The springpoint data for this glass sphere are presented in Fig. 4. Based on the diameter obtained by light scattering, the data are seen to fall on the marginal stability (springpoint) curve, indicating excellent agreement between the light-scattering technique and the springpoint method.

The calculated and the measured values of the oscillation offset and amplitude are compared in Fig. 5 for the same glass sphere. The phase lag data are compared with the theoretical predictions in Fig. 6. The data in both figures were taken at various dc voltages and are plotted against $(V_{\text{dc}}/V_{\text{dc},0} - 1)$, which is the fraction of the particle weight that is not balanced by the dc field and is directly proportional to the imbalance parameter σ . The theoretical calculations were based on $d_p = 21.9 \mu\text{m}$ from the light-scattering measurements. The offset and amplitude data are in good agreement with the continued fractions solutions. Note that both the offset and the amplitude vary linearly with the dc voltage as predicted by theory. The agreement between the measured phase lag and the theory is also

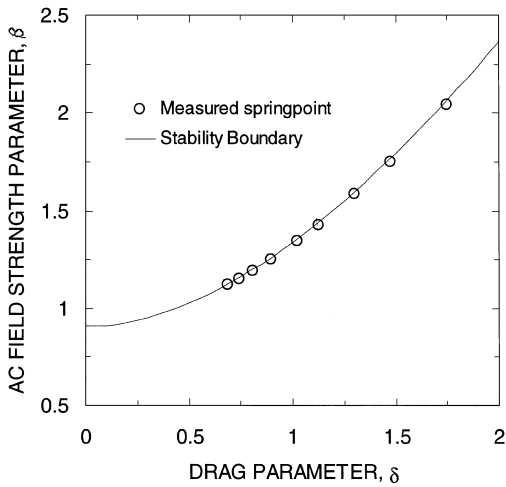


Fig. 4. Comparison of the measured and the predicted springpoints for glass sphere SLG914A.

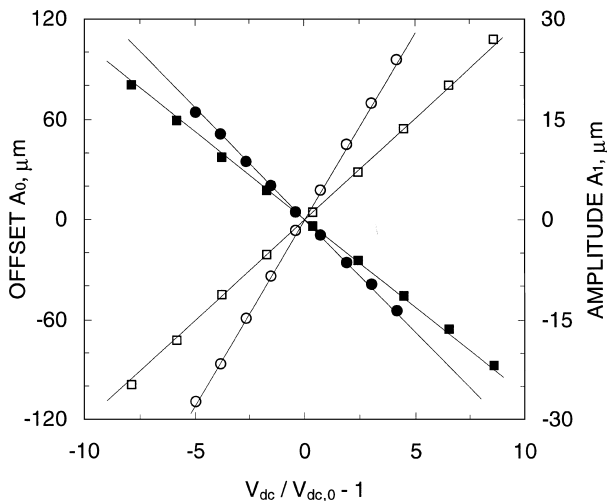


Fig. 5. Comparison of the measured and the predicted oscillation offsets and amplitudes: (○) measured offset and (●) measured amplitude for glass sphere SLG914A; (□) measured offset and (■) measured amplitude for GeO_2 particle GDO926A; (—) theoretical predictions.

good, but there is larger spread in the data, which was caused by the noise in the timing circuits of the EDB power supply. With a new design of the power supply, this error can be significantly reduced.

The diameter of the glass sphere was also determined by fitting the measured offset, the amplitude and the phase data independently to the theory. The best-fit diameters are listed in Table 1. The results for a polystyrene latex (PSL) sphere are also compared in the same table. For these spherical particles the diameters determined from particle oscillation data are within 3.9% of the light-scattering diameter and within 2.8% of the springpoint diameter.

Non-spherical particle size measurements

The non-spherical particles investigated were crystalline germanium dioxide, which are used in the production of optical fibers. Light-scattering data for these non-spherical

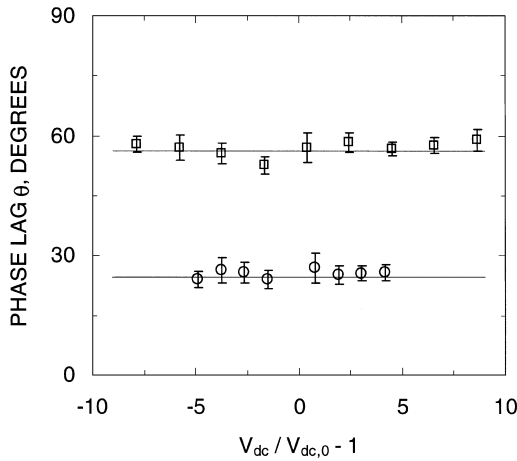
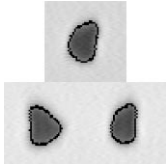


Fig. 6. Comparison of the measured and the predicted oscillation phase lags; (○) measured phase lag for glass sphere SLG914A; (□) measured phase lag for GeO_2 particle GDO926A; (—) theoretical predictions.

Table 1. Measured particle sizes and shapes

Particle ID	SLG914A	PSL904A	GDO926A	GDO930A
Particle images*				
Material	Glass	PSL	GeO_2	GeO_2
Shape	Sphere	Sphere	Oblate spheroid	Oblate spheroid
Axis ratio, q	N/A	N/A	0.67	0.65
Orientation†	N/A	N/A	90°	90°
Dynamic shape factor	N/A	N/A	0.988	0.989
d_p By offset	$21.5 \pm 0.5 \mu\text{m}$	$17.5 \pm 0.3 \mu\text{m}$	$11.7 \pm 0.1 \mu\text{m}$	$11.2 \pm 0.1 \mu\text{m}$
By amplitude	$21.8 \pm 0.5 \mu\text{m}$	$17.3 \pm 0.3 \mu\text{m}$	$12.2 \pm 0.2 \mu\text{m}$	$11.3 \pm 0.4 \mu\text{m}$
By phase	$21.5 \pm 0.5 \mu\text{m}$	$17.3 \pm 0.4 \mu\text{m}$	$11.5 \pm 0.6 \mu\text{m}$	$10.8 \pm 1.5 \mu\text{m}$
By springpoint	$22.1 \pm 0.2 \mu\text{m}$	$17.6 \pm 0.2 \mu\text{m}$	$11.8 \pm 0.2 \mu\text{m}$	N/A
By light sca.	$21.9 \pm 0.1 \mu\text{m}$	$18.0 \pm 0.1 \mu\text{m}$	N/A	N/A

*The edges were enhanced by image processing.

†The angle between the axis of revolution of the spheroid and the direction of the oscillation.

particles cannot be interpreted using conventional Mie theory. Therefore, only spring-points, oscillation offsets, amplitudes and phase lags were measured.

The axis ratios of the individual particles were determined by analyzing the video images. Two images of particle GDO926A and three images of particle GDO930A are shown in Table 1. These images were among those obtained by altering the ac frequency and amplitude to produce some rotation in the horizontal plane, that is, rotation about the vertical axis. Both particles were modeled as oblate spheroids aligned with their axes of revolution in the horizontal direction. The particles remained in the same orientation without rotation during the oscillation measurements. With the knowledge of both axis ratios and particle orientations, the dynamic shape factors were calculated. The results for the two GeO_2 particles are presented in Table 1.

The measured oscillation offset and amplitude are compared with the theoretical predictions for GeO_2 particle GDO926A in Fig. 5. The measured and the predicted phase lags for the same particle are compared in Fig. 6. The computed results are based on the equivalent-volume diameter determined by springpoint measurements, $d_p = 11.8 \mu\text{m}$. Theory and experiment are in good agreement for the offset and amplitude, but the results for the phase lag are less satisfactory.

Letting the equivalent-volume diameter, d_p , be a free parameter in the computations, we obtained the “best fit” results listed in Table 1. For particle GDO926A the diameters obtained from oscillation measurements are within 3.4% of the springpoint value. The charge-to-mass ratio of the other particle (GDO930A) happened to be such that it was too stable to reach the springpoint in the ac voltage range of the EDB. However, stable oscillation measurements were easy to make for this particle. The various methods scatter about a mean value of $11.1 \mu\text{m}$ by only about $\pm 2.7\%$, although the best-fit diameter using the phase lag data has a standard deviation of $\pm 14\%$.

It can be seen from the results in Table 1 that the size estimates given by the stable oscillation method are consistent with those given by other methods. For spheres the oscillation method yields particle sizes within 3.9% of those by light-scattering measurements. For both spherical and non-spherical particles, the oscillation technique yields particle sizes within 3.4% of the values by the springpoint method. Unlike the light-scattering method, the stable oscillation and the springpoint methods can be applied to both spherical and non-spherical particles.

The advantage of the stable oscillation method over the springpoint method is that the latter is not always applicable because the particle charge-to-mass ratio may be such that the particle is too stable and the ac voltage required to reach the springpoint would be exceedingly high. Consequently, the springpoint method is limited by the upper limit of ac voltage that a given EDB can supply and by the gas breakdown voltage, for gas ionization will result in particle loss due to charge neutralization. Size measurements based on the oscillation offset, the amplitude and the phase lag are not limited by these constraints.

The lower limit of particle size that the stable oscillation method can resolve depends on the resolution of the particle position sensing system. Here the linescan camera has $13 \mu\text{m}$ wide pixels. Combined with the $9.45\times$ lens, the camera is able to detect a particle that has a diameter as small as $1.4 \mu\text{m}$. The actual lower limit should be somewhat smaller than this value since each pixel also has a gray-scale depth of 256 levels. The practical limit is estimated to be approximately $1 \mu\text{m}$ with the camera pixel noise taken into account. Because of diffraction and less accurate particle position sensing the shadow imaging method becomes increasingly inaccurate as the size decreases.

The error associated with the particle size measurements by the stable oscillation technique depends on the amplitude and the frequency of the EDB ac voltage. Smaller amplitudes or higher frequencies result in a lower effective ac field strength (lower β). The oscillation offset and the amplitude are more sensitive to the particle size at lower values of β . This can be clearly seen in Figs. 7 and 8, in which the dimensionless oscillation offset and amplitude, respectively, are plotted against the drag parameter. Consequently, particle size measurements based on the oscillation offset and amplitude data should be carried out at low ac voltage. On the other hand, it can be seen in Fig. 9 that the sensitivity of the oscillation phase lag to the drag parameter depends only weakly on the ac field strength. This is an advantage of the phase lag method because strong ac fields can be applied to trap the particle more stably and therefore to minimize the effects of gas convection and particle Brownian motion. However, accurate phase lag measurements impose stricter requirements on the equipment than the oscillation offset and amplitude measurements because the particle position sensing must be synchronized with the ac field.

The shape and orientation of non-spherical particles also affect the accuracy of the size measurements. In this work the non-spherical GeO_2 particles were approximated as spheroids. The deviation of the actual shapes from those of spheroids becomes a source of error in estimating the particle size. It is difficult to estimate the amount of error associated with the shape deviation from spheroidal in the fitted diameters listed in Table 1 because

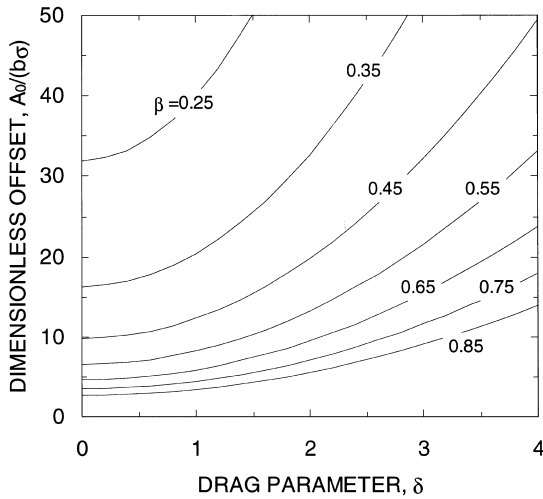


Fig. 7. The Effect of the ac field strength parameter and the drag parameter on the oscillation offset.

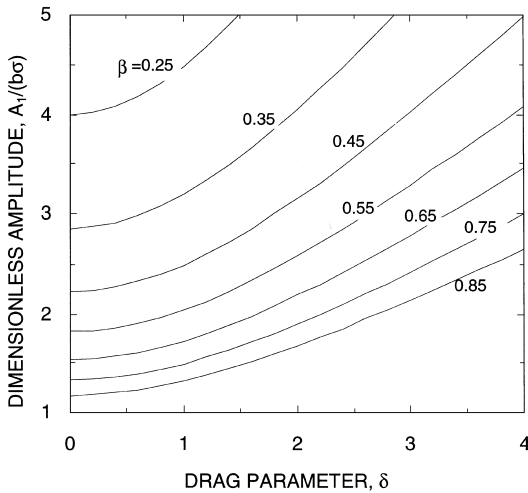


Fig. 8. The effect of the ac field strength parameter and the drag parameter on the oscillation amplitude.

theoretical dynamic shape factors are not available for arbitrary geometries. To provide an estimate of this error we analyzed a sequence of about 10 images for each particle and reconstructed the particle volume based on these cross sections. From this analysis the spheroid approximations associated with Table 1 underestimate the volume of particle GDO926A by -0.2% and overestimate that of particle GDO930A by 14.4% . The corresponding errors in the effective diameter, d_p , are -0.1 and 4.6% , respectively.

As mentioned above, spheroids usually can be made to remain in the same orientation during the oscillation measurements. However, for particles with highly irregular shapes this becomes difficult. The particles may start to vibrate between several relatively stable orientations. In this case the uncertainty in particle orientation becomes another source of error in the particle size determination.

CONCLUSIONS

We have shown that particle oscillation measurements can be used to determine the particle size to within 3.9% of the light-scattering size for spheres. The oscillation

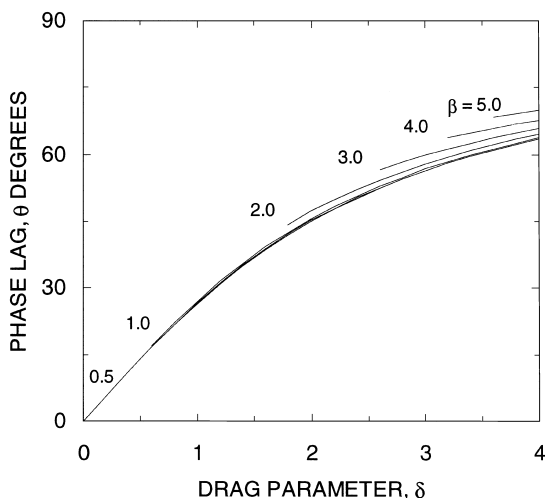


Fig. 9. The effect of the ac field strength parameter and the drag parameter on the oscillation phase lag.

measurements yield particle size estimates within 2.8% of the values obtained by the springpoint method for spherical particles and within 3.4% for the non-spherical GeO_2 particles. The oscillation method can be applied to non-spherical particles and it can be applied to particles for which springpoints are impossible to reach.

The lower limit of particle diameter that can be measured using the oscillation technique is estimated to be around $1\ \mu\text{m}$ with the apparatus used in this work. The accuracy of the oscillation size measurements can be improved by using a relatively weak ac field. For non-spherical particles the uncertainty in shape and orientation contribute to the error in the particle size estimates.

Acknowledgements—The authors are grateful to NASA for Grant NAG3-1837 that supported this research.

REFERENCES

- Aardahl, C. L., Vehring, R., Davis, E. J., Schweiger, G. and Swanson, B. D. (1997a) Trapping two-particle arrays in a double-ring electrodynamic balance. *J. Aerosol Sci.* **28**, 1491–1505.
- Aardahl, C. L., Vehring, R., Weber, R., Schweiger, G., Davis, E. J. and Wiedensohler, A. (1997b) Electrodynamic trapping of aerocolloidal particles: experimental and theoretical trapping limits. *J. Colloid Interface Sci.* **192**, 228–237.
- Ataman, S. and Hanson, D. N. (1969) Measurement of charged drops. *Ind. Eng. Chem. Fundam.* **8**, 833–836.
- Bar-Ziv, E. and de Botton, G. (1991) The motion of a charged particle in an electrodynamic chamber under feedback control. *Aerosol Sci. Technol.* **15**, 1–7.
- Blau, H. H., McCleese, D. J. and Watson, D. (1970) Scattering by individual transparent spheres. *Appl. Opt.* **9**, 2522–2528.
- Davis, E. J. (1985) Electrodynamic balance stability characteristics and applications to the study of aerocolloidal particles. *Langmuir* **1**, 379–387.
- Davis, E. J. and Periasamy, R. (1985) Light scattering and aerodynamic size measurements for homogeneous and inhomogeneous microspheres. *Langmuir* **1**, 373–379.
- Davis, E. J. and Ray, A. K. (1980) Single aerosol particle size and mass measurements using an electrodynamic balance. *J. Colloid Interface Sci.* **75**, 566–576.
- Frickel, R. H., Shaffer, R. E. and Stamatoff, J. B. (1978) Report No. ARCSL-TR-77041, Chemical Systems Laboratory, Aberdeen Proving Ground, MD.
- Göbel, G., Wriedt, T. and Bauckhage, K. (1997) Periodic drag force and particle size measurement in a double ring electrodynamic trap. *Rev. Sci. Instrum.* **68**, 3046–3052.
- Gucker, F. T. and Egan, J. J. (1961) Measurement of the angular variation of light scattered from single aerosol droplets. *J. Colloid Sci.* **16**, 68–84.
- Kasper, G. (1982) Dynamics and measurement of smokes. 1. Size characterization of non-spherical particles. *Aerosol Sci. Technol.* **1**, 187–199.
- Laucks, M. L., Roll, G., Schweiger, G. and Davis, E. J. (2000) Physical and chemical (Raman) characterization of bioaerosols—pollen. *J. Aerosol Sci.* **31**, 307–319.

- Li, W. and Davis, E. J. (1995) Measurement of the thermophoretic force by electrodynamic levitation: microspheres in air. *J. Aerosol Sci.* **26**, 1063–1083.
- Maloney, D. J., Lawson, L. O., Fasching, E. G. and Monazam, E. R. (1995) Measurement and dynamic simulation of particle trajectories in an electrodynamic balance: characterization of particle drag force coefficient/mass ratios. *Rev. Sci. Instrum.* **66**, 3615–3622.
- Müller, A. (1960) Theoretische untersuchungen über das verhalten geladener teilchen in sattelpunkten electrischer wechselfelder. *Ann. Phys.* **6**, 206–220.
- Oberbeck, A. (1876) On stationary fluid motions when viscosity is taken into consideration. *J. Math.* **81**, 62.
- Rassat, S. D. and Davis, E. J. (1992) Chemical reaction between sulfur dioxide and a calcium oxide aerosol particle. *J. Aerosol Sci.* **23**, 765–780.
- Roll, G., Kaiser, T. and Schweiger, G. (1996) Optical trap sedimentation cell—A new technique for the sizing of microparticles. *J. Aerosol Sci.* **27**, 105–117.
- Sageev, G., Seinfeld, J. H. and Flagan, R. C. (1986) Particle sizing in the electrodynamic balance. *Rev. Sci. Instrum.* **57**, 933–936.
- Swanson, B. D., Bacon, N. J., Davis, E. J. and Baker, M. B. (1999) Electrodynamic trapping and manipulation of ice crystals. *Q. J. Roy. Meteorol. Soc.* **125**, 1039–1055.
- Taflin, D. C., Ward, T. L. and Davis, E. J. (1989) Electrified droplet fission and the Rayleigh limit. *Langmuir* **5**, 376–384.